



---

## Figures and figure supplements

Expression of WIPI2B counteracts age-related decline in autophagosome biogenesis in neurons

**Andrea KH Stavoe et al**

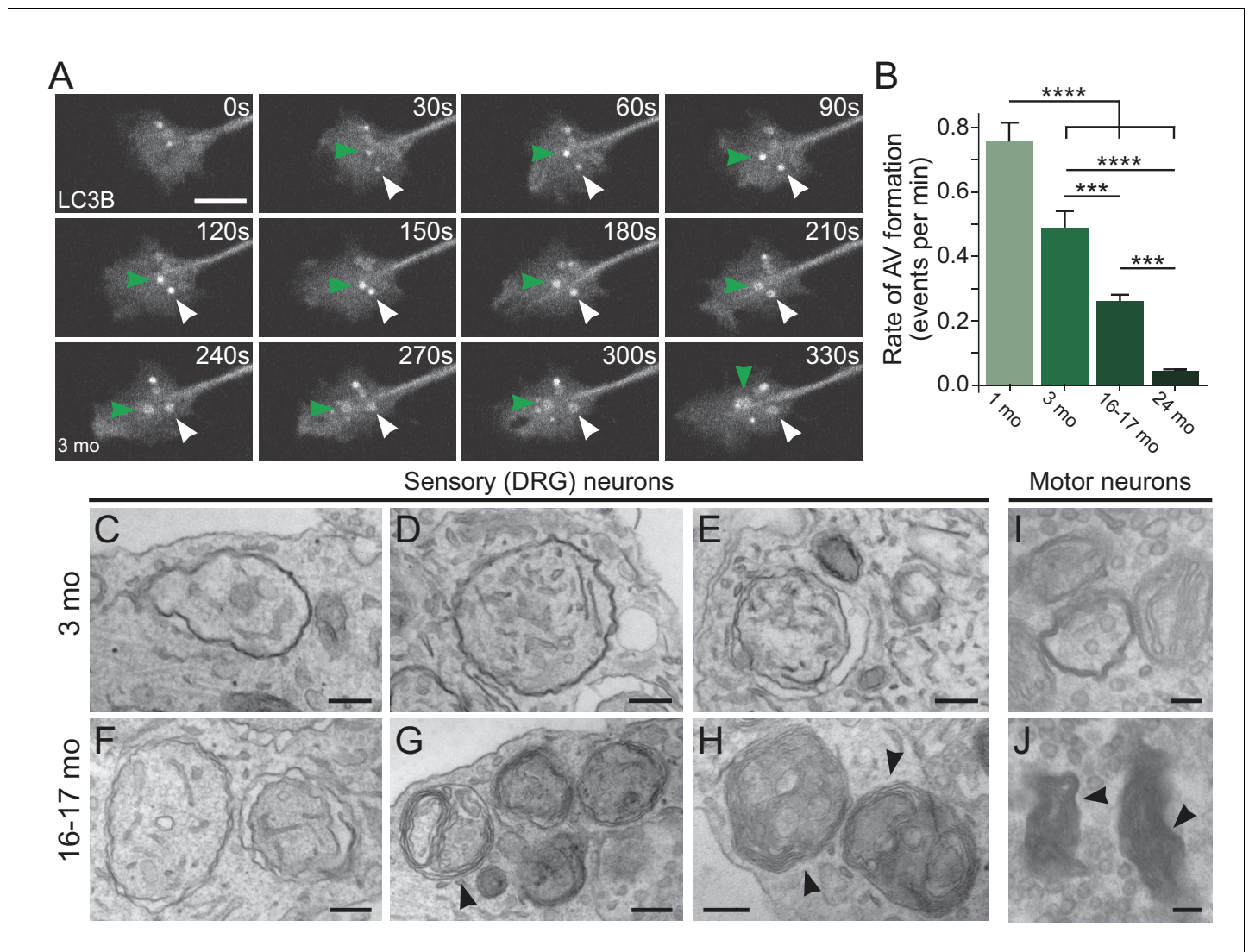


**Figure 1.** Autophagosome biogenesis decreases with age and results in aberrant AV formation in mammalian neurons. **(A)** Time series of GFP-LC3B in the distal axon of a DRG neuron from a young adult mouse. Green and white arrowheads each follow one autophagosome biogenesis event. Retrograde is to the right. Scale bar, 2  $\mu$ m. **(B)** Quantification of the rate of autophagic vesicle (AV) biogenesis (assayed by GFP-LC3B puncta formation per minute) in DRG neurons from young (one mo, light green), young adult (three mo, green), aged (16–17 mo, dark green), and advanced aged (24 mo, very dark green) mice (mean  $\pm$  SEM;  $n \geq 54$  neurons from three biological replicates). \*\*\* $p < 0.0005$ ; \*\*\*\* $p < 0.0001$  by one-way ANOVA test with Tukey's multiple comparisons test. **(C–E)** Representative electron micrographs of autophagosomes in DRG distal tips from young adult mice. AVs are composed of a continuous double membrane enclosing engulfed cytoplasm. Scale bars, 200 nm. **(F–H)** Representative electron micrographs of autophagosomes in DRG distal tips from aged mice. AVs contain multiple, ruffled double membranes (**G**, **H**). Scale bars, 200 nm. **(I–J)** Electron micrographs of autophagosomes in the presynaptic compartment of neuromuscular junctions (NMJs) from young adult (**I**) and aged (**J**) mice. Scale bars, 100 nm. Arrowheads indicate multilamellar membranes in DRGs and NMJs.

DOI: <https://doi.org/10.7554/eLife.44219.003>

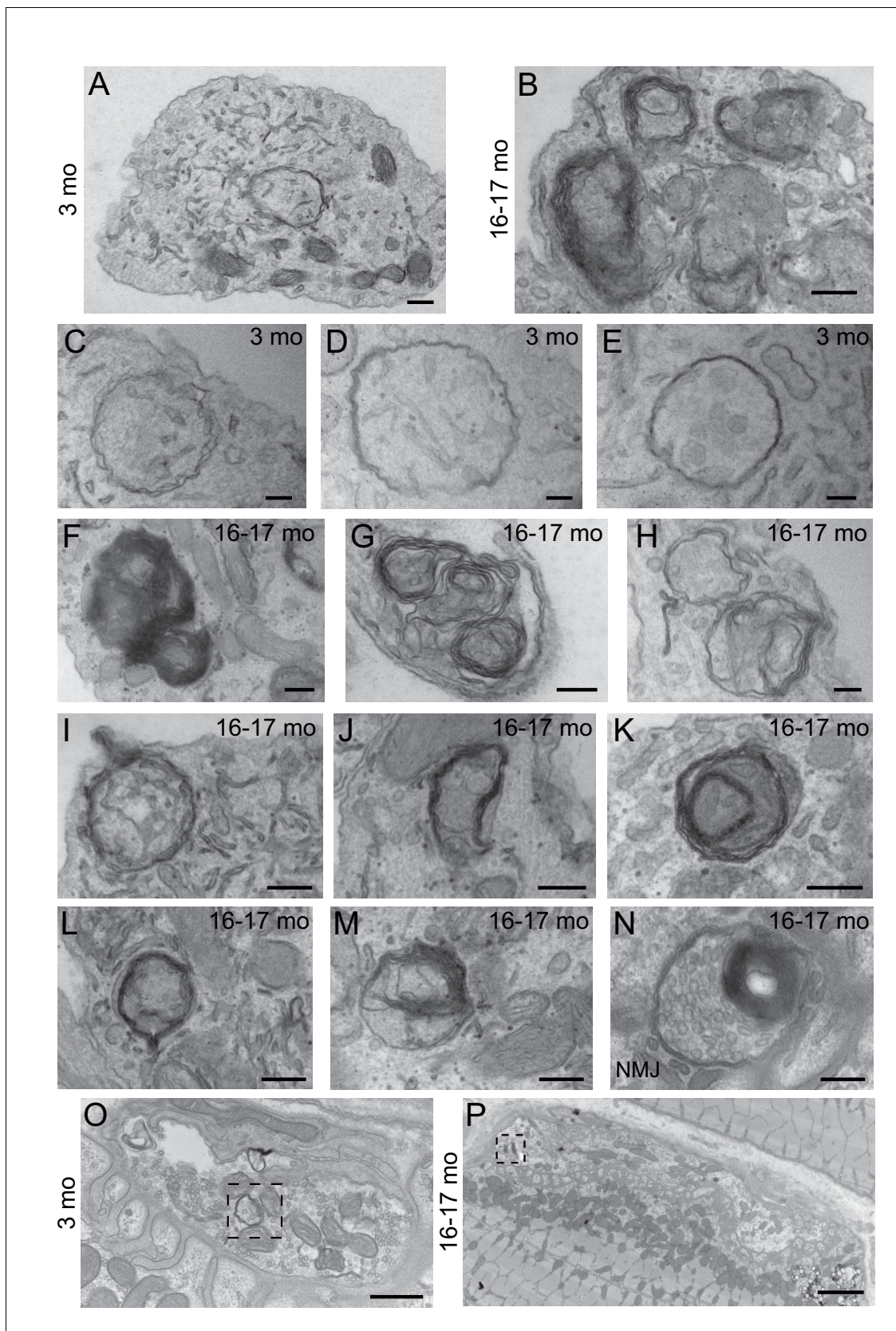


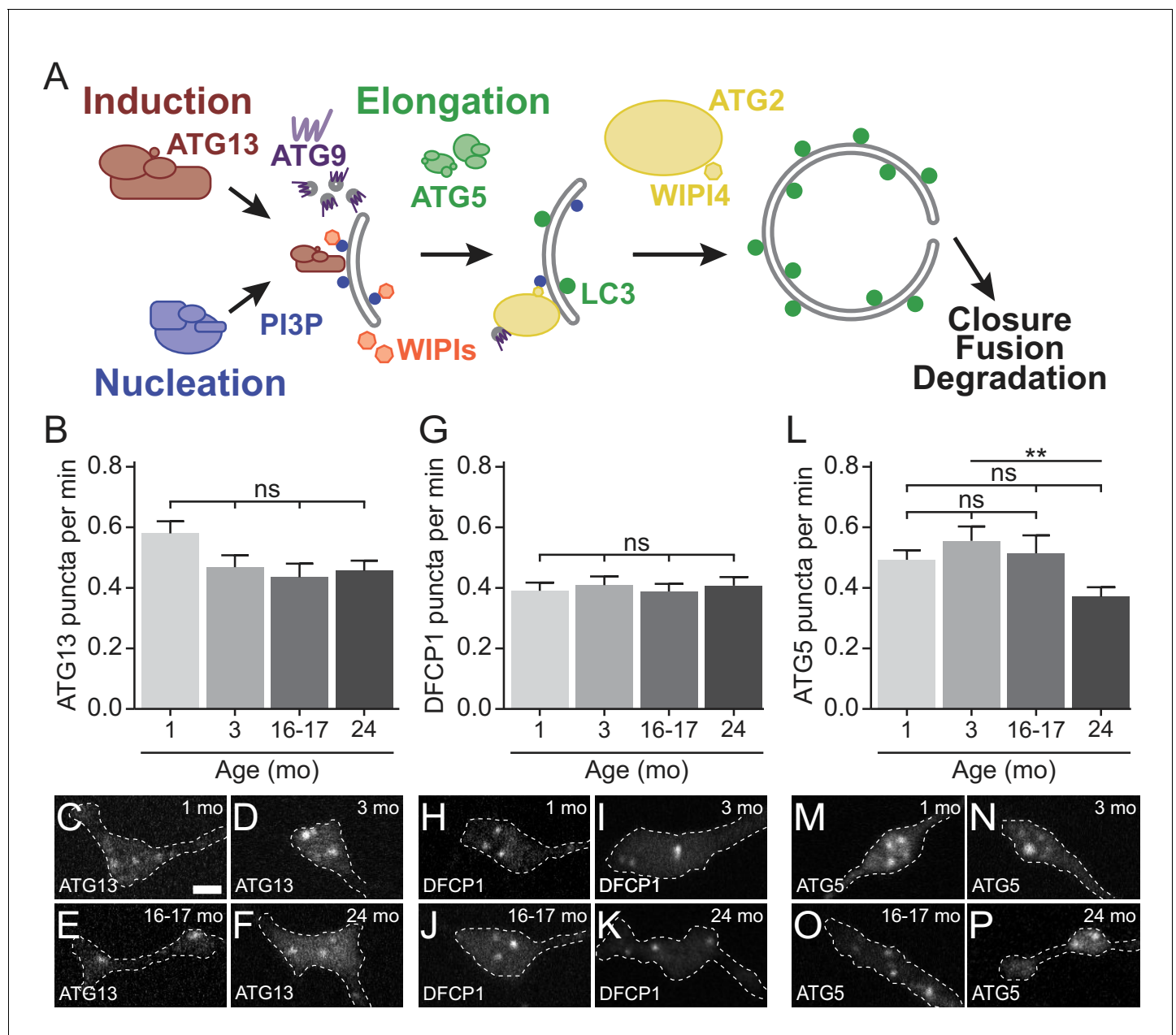
**Figure 1—figure supplement 1.** Morphological differences in autophagosomes in neurons from young adult and aged mice. (A–B) Electron micrographs of DRG distal tips from young adult (A) or aged (B) mice. Scale bars, 200 nm. (C–E) Representative electron micrographs of Figure 1—figure supplement 1 continued on next page

*Figure 1—figure supplement 1 continued*

autophagosomes in DRG axonal distal tips from young adult mice. Scale bars, 200 nm. (**F–M**) Representative electron micrographs of autophagosomes in DRG axonal distal tips from aged mice. Scale bars, 200 nm. (**N**) Representative electron micrograph of an autophagosome in a NMJ from an aged mouse. Scale bar, 200 nm. (**O–P**) Lower magnification electron micrographs of **Figure 1I and J** of autophagosomes in the presynaptic compartment of NMJs from young adult (**O**) and aged (**P**) mice. Dashed boxes indicate corresponding magnified regions in **Figure 1I–1J**. Scale bar in O, 500 nm; in P, 2  $\mu$ m.

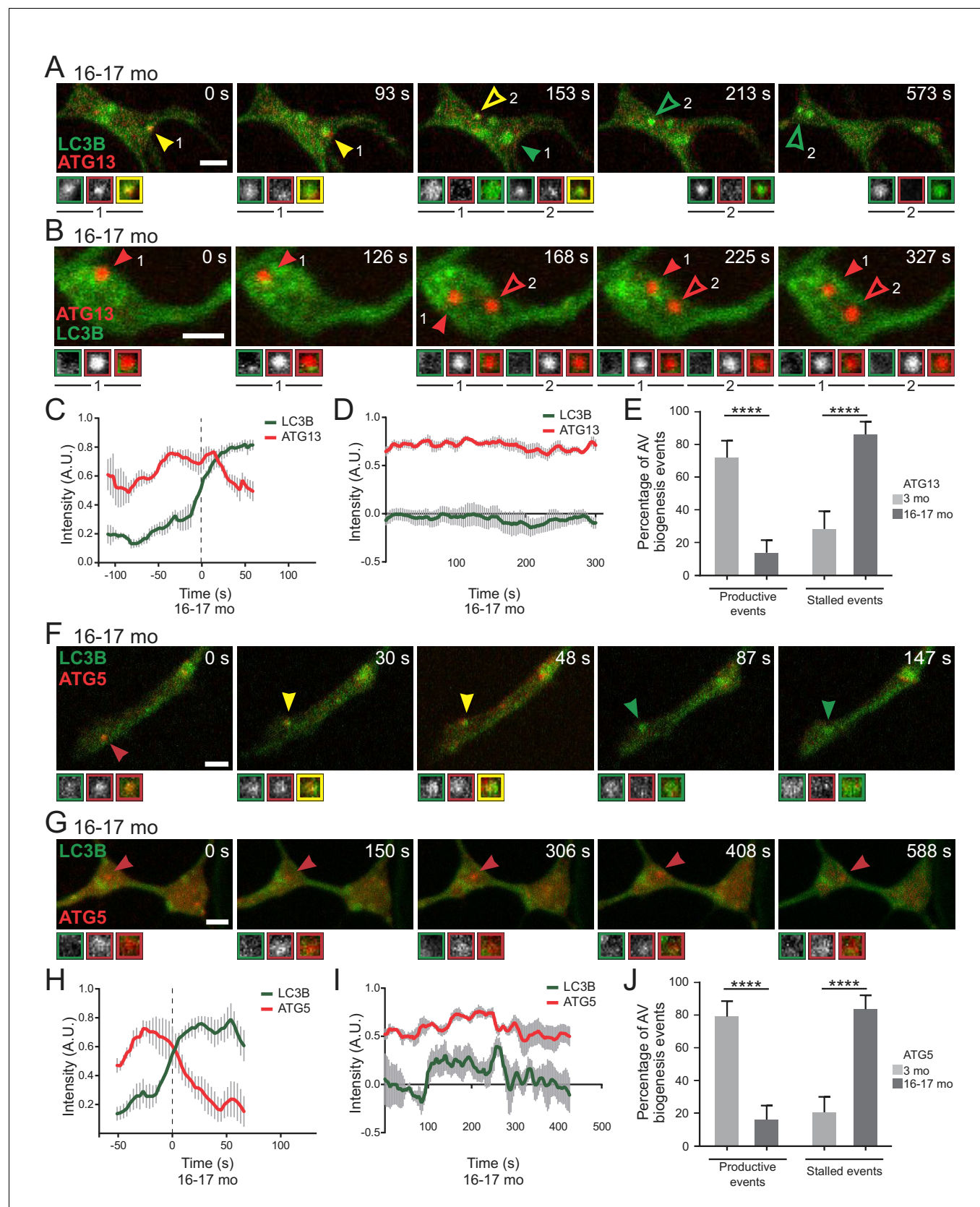
DOI: <https://doi.org/10.7554/eLife.44219.004>





**Figure 2.** Early autophagosome biogenesis components do not change with age. **(A)** Schematic of autophagy pathway, focusing on the protein complexes involved in autophagosome biogenesis: induction (red), nucleation (blue), elongation (green), and ATG2/WIPI4 (yellow). ATG9, a multi-pass transmembrane protein is in purple. The product of the nucleation complex, PI3P, is depicted as a blue dot, while LC3-II, the product of the elongation complex, is depicted as a green dot. WIPI1 and WIPI2, which bind to PI3P, are displayed in orange. **(B–F)** Quantification of the rate of mCh-ATG13 puncta formation in live-cell imaging of DRG neurons from young, young adult, aged, and advanced aged mice (mean  $\pm$  SEM;  $n \geq 28$  neurons from three biological replicates). ns, not significant by Kruskal-Wallis ANOVA test with Dunn's multiple comparisons test. **(C–F)** Representative micrographs of mCh-ATG13 in the distal tip of DRG neurons from young (C), young adult (D), aged (E), and advanced aged (F) mice. **(G)** Quantification of the rate of Halo-DFCP1 puncta in DRG neurons from young, young adult, aged, and advanced aged mice (mean  $\pm$  SEM;  $n \geq 18$  neurons from three biological replicates). ns, not significant by Kruskal-Wallis ANOVA test with Dunn's multiple comparisons test. **(H–K)** Representative micrographs of Halo-DFCP1 in the distal tip of DRG neurons from young (H), young adult (I), aged (J), and advanced aged (K) mice. **(L)** Quantification of the rate of mCh-ATG5 puncta in DRG neurons from young, young adult, aged, and advanced aged mice (mean  $\pm$  SEM;  $n \geq 34$  neurons from three biological replicates). ns, not significant; \*\* $p < 0.001$  by Kruskal-Wallis ANOVA test with Dunn's multiple comparisons test. **(M–P)** Representative micrographs of mCh-ATG5 in the distal tip of DRG neurons from young (M), young adult (N), aged (O), and advanced aged (P) mice. Scale bar in C, 2  $\mu$ m, for C–F, H–K, M–P.

DOI: <https://doi.org/10.7554/eLife.44219.005>



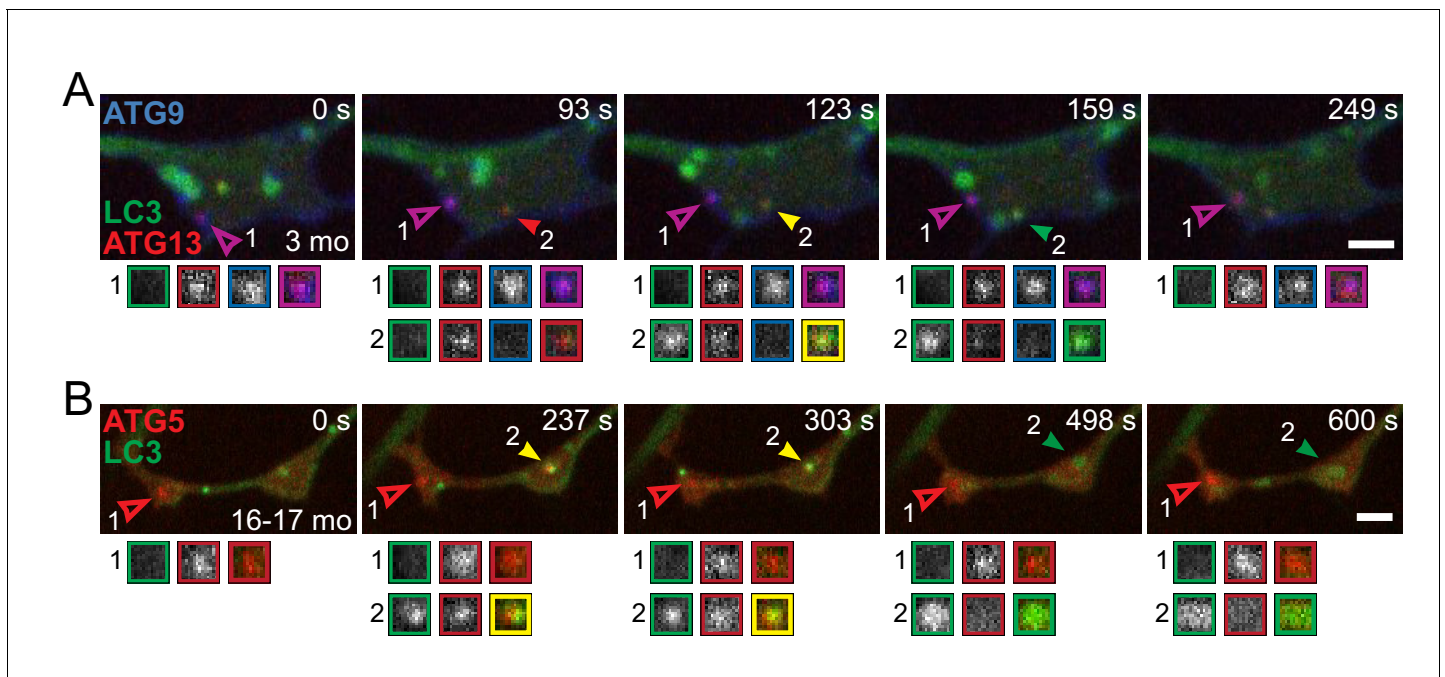
**Figure 3.** Stalled AVs predominate in neurons from aged mice. (A–B) Time series of merge micrographs of mCh-ATG13 and GFP-LC3B from live cell imaging of the distal neurite of DRGs from aged mice depicting a productive (A) or a stalled (B) autophagosome biogenesis event. Yellow arrowheads

Figure 3 continued on next page

## Figure 3 continued

denote colocalization of mCh-ATG13 and GFP-LC3B; green arrowheads denote a GFP-LC3B-positive punctum from which mCh-ATG13 has dissociated; red arrowheads denote mCh-ATG13-positive puncta that fail to recruit GFP-LC3B; solid arrowheads track one punctum, hollow arrowheads follow a second punctum. Magnified views of denoted puncta are shown below full micrograph; border color represents channel or colocalization state in merge. Retrograde is to the right. Scale bars, 2  $\mu$ m. (C–D) Individual intensity profiles were averaged to improve signal-to-noise of mCh-ATG13 (red) and GFP-LC3B (green) for productive (C) and stalled (D) AVs (mean  $\pm$  SEM;  $n \geq 5$  biogenesis events from five neurons from three biological replicates). (E) Quantification of the proportion of total mCh-ATG13-positive AV biogenesis events (both productive and stalled events) in DRG neurons from young adult (light gray) and aged (dark gray) mice (mean  $\pm$  95% confidence interval;  $n \geq 62$  AVs from three biological replicates for each condition). \*\*\*\* $p < 0.0001$  by Fisher's exact test. (F–G) Time series of merge micrographs of mCh-ATG5 and GFP-LC3B in the distal neurite of DRGs from aged mice depicting a productive (F) or stalled (G) autophagosome biogenesis event. Arrowheads point to puncta magnified below micrograph; colors denote channel or colocalization state in merge. Scale bars, 2  $\mu$ m. (H–J) Mean intensity profiles of mCh-ATG5 (red) and GFP-LC3B (green) for productive (H) and stalled (I) AVs (mean  $\pm$  SEM;  $n = 5$  productive biogenesis events from five neurons or  $n = 4$  stalled biogenesis events from four neurons from three biological replicates). Vertical dashed line in (C and H) indicates the half-maximum of GFP-LC3B intensity, which was used to align the traces. (J) Quantification of the proportion of total mCh-ATG5-positive AV biogenesis events (both productive and stalled events) in DRG neurons from young adult and aged mice (mean  $\pm$  95% confidence interval;  $n \geq 62$  AVs from three biological replicates for each condition). \*\*\*\* $p < 0.0001$  by Fisher's exact test. See also **Videos 1–6**.

DOI: <https://doi.org/10.7554/eLife.44219.012>



**Figure 3—figure supplement 1.** Productive and stalled AVs occur in the same axonal tips. (A) Time series of GFP-LC3B, mCh-ATG13, and SNAP-ATG9 in the distal neurite of a DRG neuron from a young adult mouse depicting a productive autophagosome biogenesis event (solid arrowhead, #2) and a stalled biogenesis event (outlined arrowhead, #1). (B) Time series of GFP-LC3B and mCh-ATG5 in the distal neurite of a DRG neuron from an aged mouse depicting a productive autophagosome biogenesis event (solid arrowhead, #2) and a stalled biogenesis event (outlined arrowhead, #1). Magnified views of denoted puncta are shown below full micrograph; border color represents channel or colocalization state in merge. Retrograde is to the right. Scale bars, 2  $\mu$ m.

DOI: <https://doi.org/10.7554/eLife.44219.013>



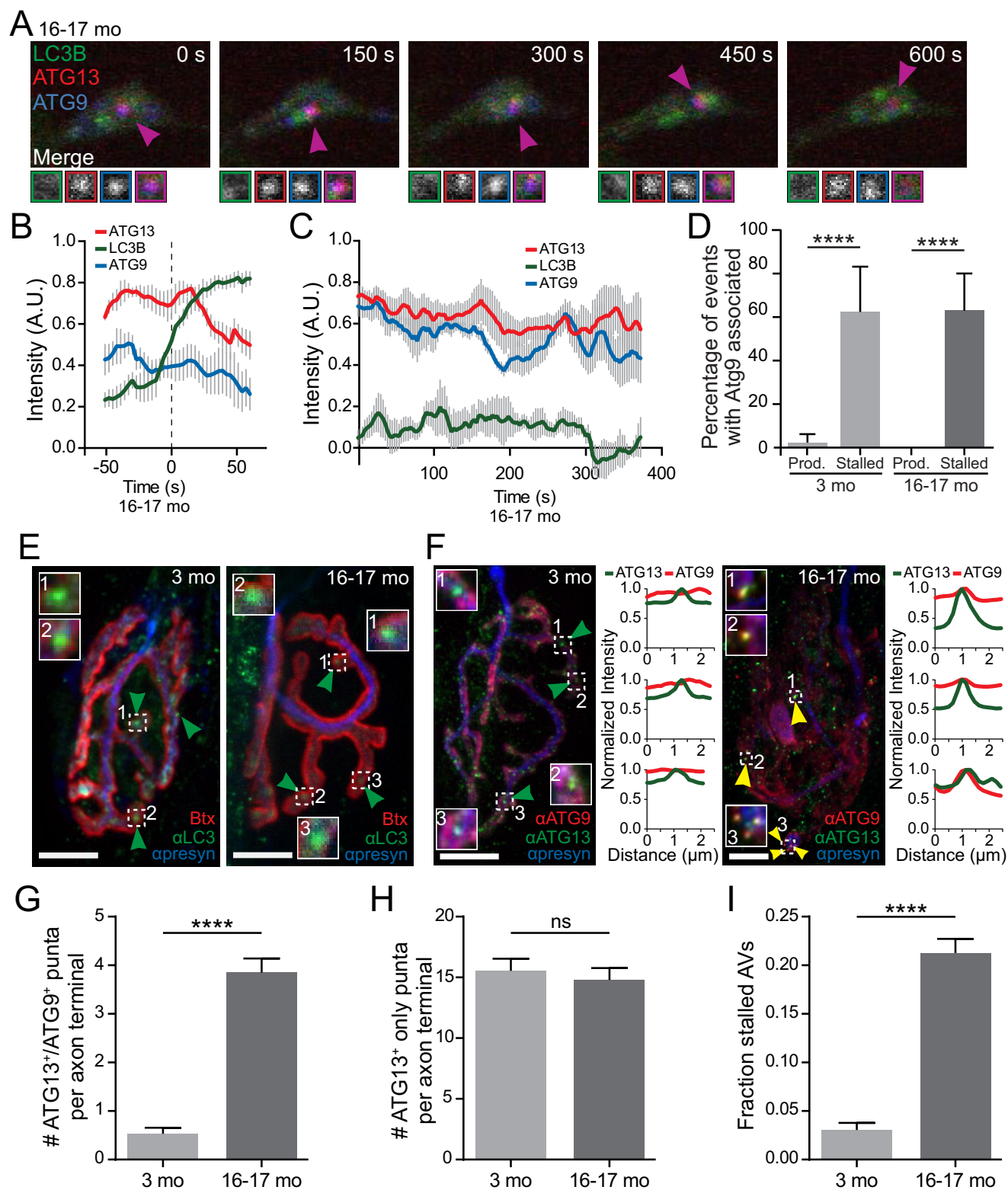


**Figure 4.** Atg9, a multi-pass transmembrane protein, aberrantly associates with stalled AVs in vitro and in vivo. (A) Time series of live imaging of mCh-ATG13, SNAP-ATG9, and GFP-LC3B in the distal neurite of a DRG neuron from an aged mouse depicting a stalled AV. Magenta arrowheads indicate

Figure 4 continued on next page

## Figure 4 continued

colocalization between mCh-ATG13 and SNAP-ATG9 without GFP-LC3B. Magnified views of denoted puncta are shown below full micrograph; border color represents channel or colocalization state in merge. Retrograde is to the right. Scale bar, 2  $\mu\text{m}$ . (B–C) Mean intensity profiles of mCh-ATG13 (red), SNAP-ATG9 (blue), and GFP-LC3B (green) for productive (B) and stalled (C) AVs in DRG distal tips from aged mice (mean  $\pm$  SEM;  $n = 5$  biogenesis events from five neurons from three biological replicates for each graph). Vertical dashed line in (B) indicates the half-maximum of GFP-LC3B intensity, which was used to align the traces. (D) Quantification of the percentage of AVs that have SNAP-ATG9 associated in the distal neurites of DRGs from young adult and aged mice (mean  $\pm$  95% confidence interval;  $n \geq 17$  for each age group). \*\*\*\* $p < 0.0001$  by two-tailed Fisher's exact test. (E–F) Maximal projection micrographs of NMJs from young adult (three mo) and aged mice (16–17 mo). In panel (E), NMJs were stained with  $\alpha$ -Bungarotoxin-tetramethylrhodamine (Btx) to stain the endplate, anti-SV2 together with anti-neurofilament H (both in blue) to visualize the presynaptic motor neuron, and anti-LC3B to visualize AVs at the synapse. In panel (F), NMJs from young and aged mice were stained with the presynaptic markers SV2 and neurofilament H (together in blue), as well as antibodies to ATG9 (red) and ATG13 (green). Dashed boxes indicate magnified insets; line scans of ATG9 (red) and ATG13 (green) intensities at the indicated puncta are also shown. Scale bars, 10  $\mu\text{m}$ . Arrowheads denote LC3B AVs (E) or the colocalization state of ATG13 with ATG9 at AVs (F). (G–I) Quantification of micrographs of NMJs from young adult (gray) and aged (dark gray) mice stained with Btx, anti-SV2, anti-neurofilament H, anti-ATG13, and anti-ATG9. (G) Quantification of stalled AVs, defined as colocalization of ATG13 and ATG9 at puncta, in the NMJ motor axon terminal. (H) Quantification of ATG13 puncta that do not have colocalized ATG9 in the NMJ motor axon terminal. (I) Quantification of the fraction of stalled AVs out of the total ATG13-positive puncta in the NMJ motor axon terminal. In G–I, mean  $\pm$  SEM;  $n \geq 62$  motor axon terminals for each age from three biological replicates. \*\*\*\* $p < 0.0001$ , ns = 0.3443 by Mann-Whitney t tests. See also **Videos 3,4,7**. DOI: <https://doi.org/10.7554/eLife.44219.015>

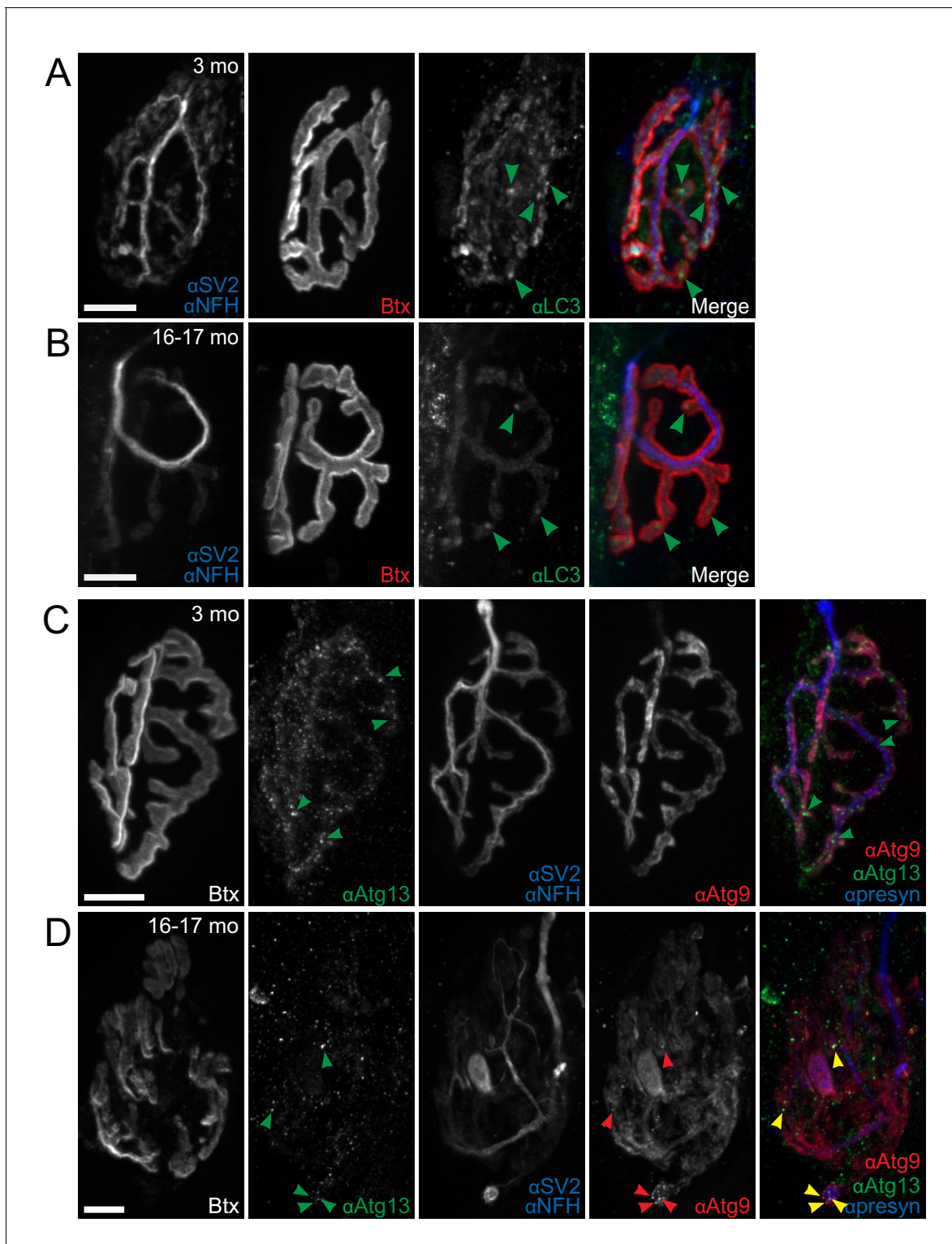


**Figure 4—figure supplement 1.** NMJ immunohistochemistry. (A–D) Individual channels of maximal projection micrographs of NMJs from young adult (three mo) and aged mice (16–17 mo) shown in **Figure 4E–F**. (A–B), NMJs were stained with  $\alpha$ - Btx to stain the endplate, anti-SV2 together with anti-neurofilament H (NFH) (both in blue) to visualize the presynaptic motor neuron, and anti-LC3B to visualize AVs at the synapse. (C–D), NMJs from young and aged mice were stained with the anti-SV2 and anti-NFH (together in blue), as well as anti- ATG9 and anti-ATG13. Scale bars, 10  $\mu$ m. Arrowheads denote LC3B AVs (A–B) or the colocalization state of ATG13 with ATG9 at AVs (C–D). Merge micrographs are the same as in **Figure 4E–F**.

DOI: <https://doi.org/10.7554/eLife.44219.016>

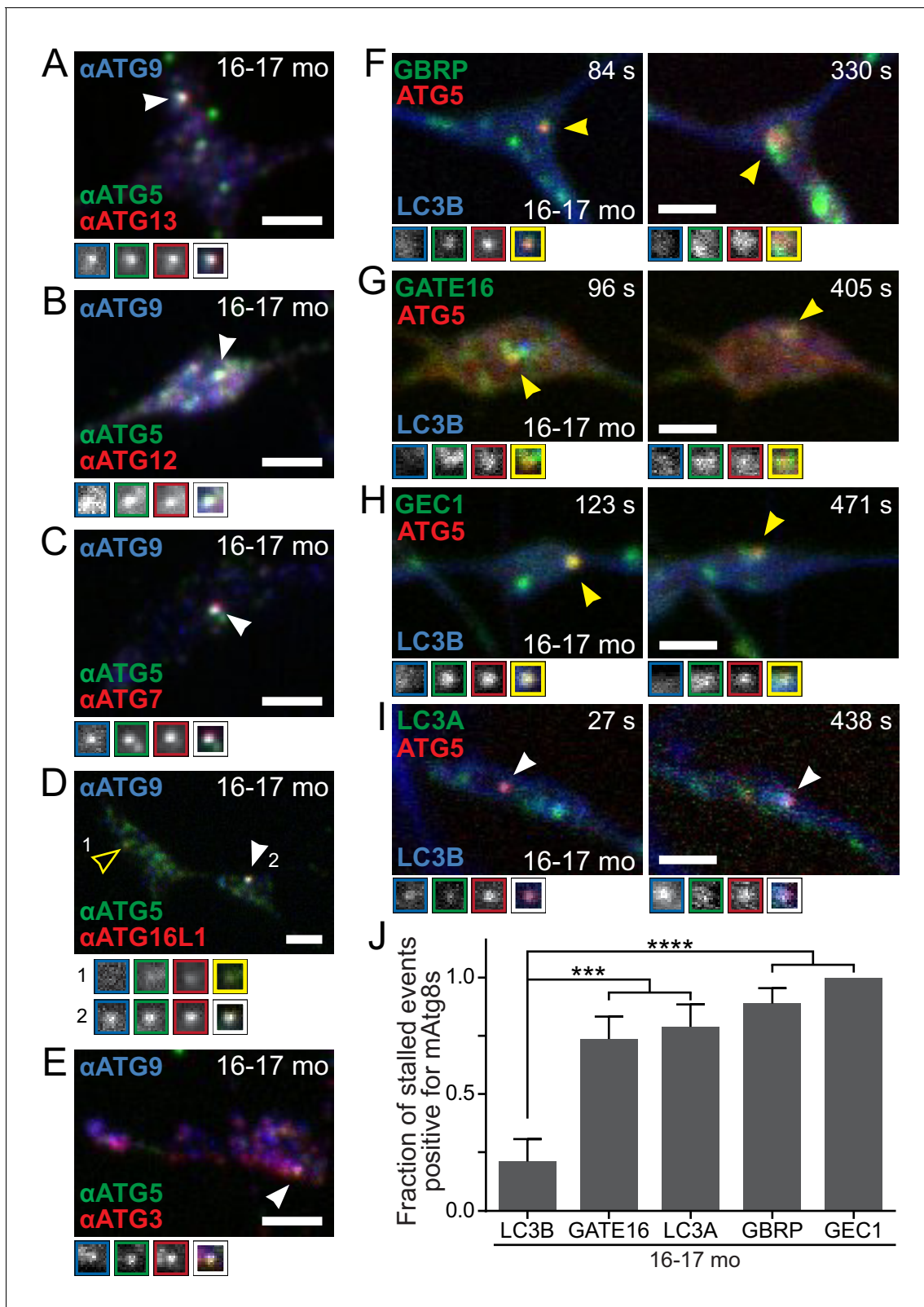


**Figure 5.** Recruitment of autophagy machinery, including LC3B homologs, to stalled AVs is not sufficient to rescue the biogenesis defect. (A–E) Representative maximal projection micrographs of the distal neurites of fixed DRG neurons from aged mice. Stalled AVs are identified by colocalization of anti-ATG5 (green) and anti-ATG9 (blue). Antibodies to other autophagy components are visualized in red: ATG13 (A) or elongation complex components ATG12 (B), ATG7 (C), ATG16L1 (D), and ATG3 (E). Arrowheads denote colocalization state of AVs (stalled, filled arrowheads). Borders of Figure 5 continued on next page



*Figure 5 continued*

magnifications of indicated puncta denote channel or colocalization state in merge. (F–I) Time series (channels merged) of Halo-ATG5, mAtg8s (mCh-GABARAP in F, mCh-GABARAPL2/GATE16 in G, mCh-GABARAPL1/GEC1 in H, and mScarlet-LC3A in I), and GFP-LC3B in the distal neurite of DRG neurons from aged mice depicting stalled AVs. Arrowheads denote colocalization of mAtg8s with stalled AVs. Magnified views of denoted puncta are shown below full micrograph; border color represents channel or colocalization state in merge. Time is indicated as time since stalled AV was first visible. (J) Quantification of the fraction of stalled AVs co-recruiting each LC3/GABARAP family member when individually overexpressed in DRGs from aged mice (mean  $\pm$  SEM;  $n \geq 10$  stalled AVs in three biological replicates for each mAtg8). \*\*\* $p < 0.001$ ; \*\*\*\* $p < 0.0001$  by two-tailed Fisher's exact test. Scale bars, 2  $\mu\text{m}$ .

DOI: <https://doi.org/10.7554/eLife.44219.017>

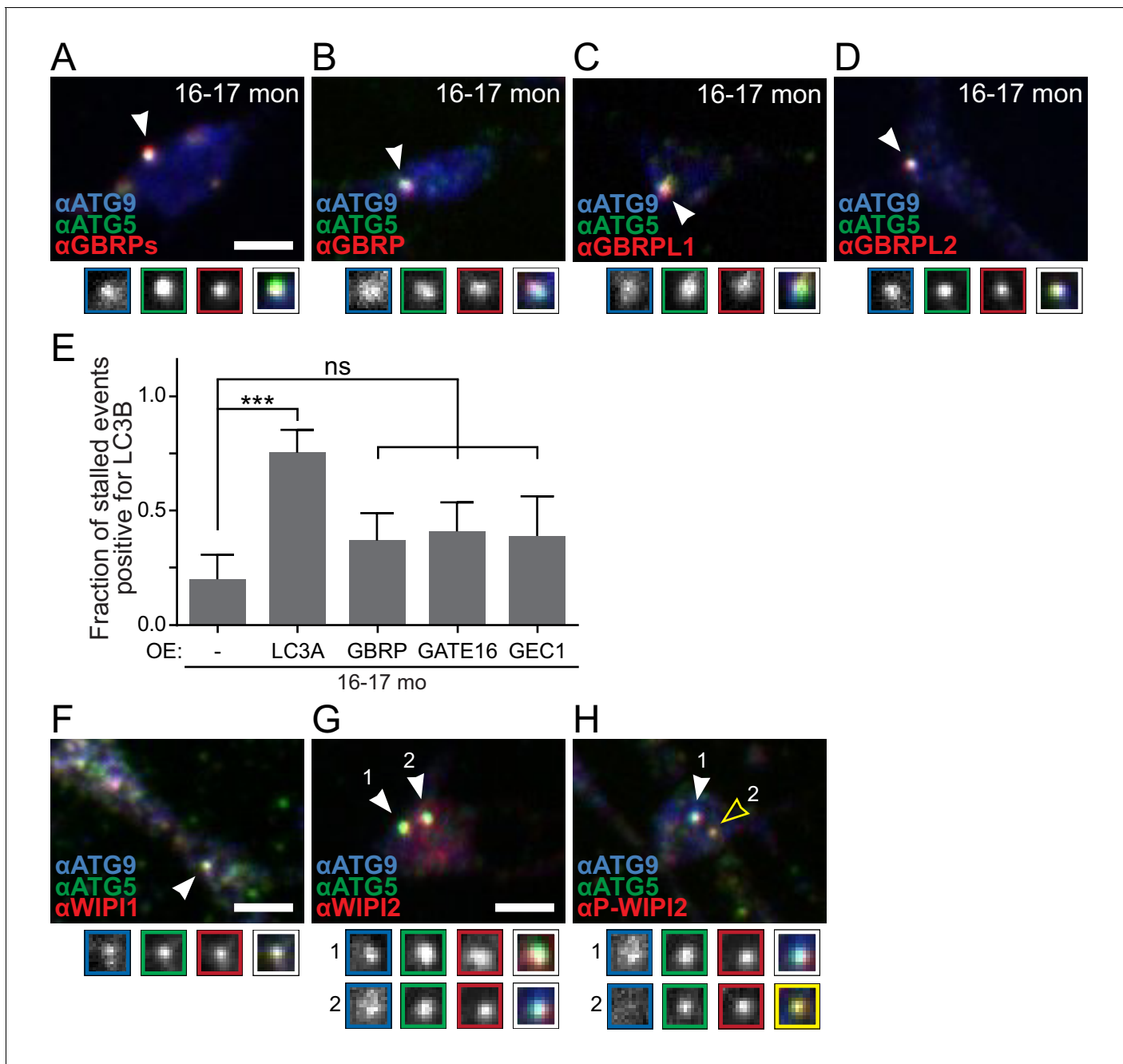


**Figure 5—figure supplement 1.** Endogenous mAtg8s are recruited to stalled AVs in vitro. (A–D) Representative maximal projection immunocytochemistry micrographs of ATG5 and ATG9 with mAtg8 homologs GABARAPs (A), GABARAP (B), GABARAPL1/GEC1 (C), and GABARAPL2/GATE-16 (D) in the distal neurites of DRG neurons from aged mice. (E) Quantification of the fraction of stalled events that are LC3B-positive in DRG neurons from aged mice with control or overexpression of individual mAtg8s (mean  $\pm$  95% confidence interval;  $n \geq 10$  AVs from three biological replicates). \*\*\* $p=0.0002$ , ns  $>0.05$  by Fisher's exact test. (F–H) Representative maximal projection immunocytochemistry micrographs of ATG5 and ATG9 with WIPI1 (F), WIPI2 (G), and phospho-WIPI2 (H). Arrowheads denote colocalization state of AVs. Magnified views of denoted puncta are shown below full micrograph; border color represents channel or colocalization state in merge. Scale bar, 2  $\mu$ m for all panels.

DOI: <https://doi.org/10.7554/eLife.44219.018>

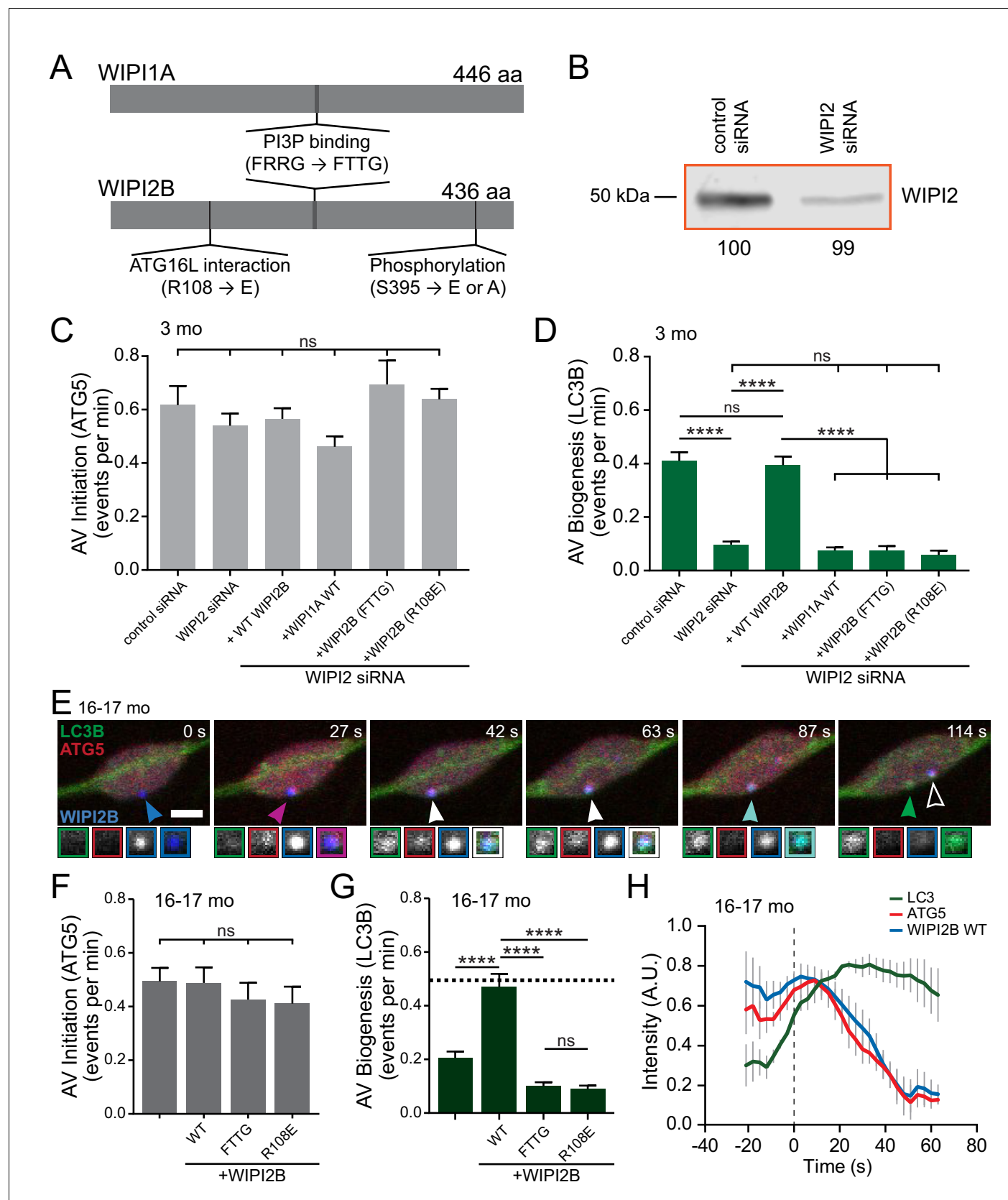


**Figure 6.** Overexpression of WIPI2B in neurons from aged mice returns autophagosome biogenesis to levels observed in neurons from young adult mice. (A) Schematic of WIPI1A and WIPI2B proteins, depicting the PI3P-interaction domains (FRRG), the ATG16L1-binding domain in WIPI2B (R108), and Figure 6 continued on next page

## Figure 6 continued

the phosphorylation site in WIP12B (S395). Point mutations to disrupt these interactions are indicated in the relevant domains (FRRG → FTTG, R108 → E, or S395 → E or A). (B) Immunoblot of DRG lysates treated with indicated siRNA, collected after 2 days in vitro. Total protein was used as a loading control; normalization factor is indicated below blot as a percentage. (C) Quantification of the rate of AV initiation (mCh-ATG5 puncta) in DRG neurons from young adult mice with control or WIP12 siRNA or WIP12 siRNA with indicated RNAi-resistant Halo-WIP12B or SNAP-WIP11A constructs (mean ± SEM;  $n \geq 15$  neurons from three biological replicates for each siRNA condition). ns (not significant)  $p > 0.05$  by Kruskal-Wallis ANOVA test with Dunn's multiple comparisons test. (D) Quantification of the rate of AV biogenesis (GFP-LC3B puncta) in DRG neurons from young adult mice with control or WIP12 siRNA or WIP12 siRNA with indicated RNAi-resistant Halo-WIP12B or SNAP-WIP11A constructs (mean ± SEM;  $n \geq 15$  neurons from three biological replicates for each siRNA condition). ns  $p > 0.05$ ; \*\*\*\* $p < 0.0001$  by Kruskal-Wallis ANOVA test with Dunn's multiple comparisons test. (E) Time series of merged micrographs of GFP-LC3B, mCh-ATG5, and Halo-WIP12B WT in the distal neurite of a DRG neuron from an aged mouse depicting a productive autophagosome biogenesis event. Arrowheads indicate colocalization state on the isolation membrane; solid arrowhead follows one punctum, while outlined arrowhead indicates a different AV biogenesis event. Magnified views of denoted puncta are shown below full micrograph; border color represents channel or colocalization state in merge. Retrograde is to the right. Scale bar, 2  $\mu\text{m}$ . (F) Quantification of the rate of AV initiation (mCh-ATG5 puncta) in DRG neurons from aged mice with or without overexpression of the indicated Halo-WIP12B construct (mean ± SEM;  $n \geq 17$  neurons from three biological replicates for each condition). ns  $p > 0.05$  by Kruskal-Wallis ANOVA test with Dunn's multiple comparisons test. (G) Quantification of the rate of AV biogenesis (marked with GFP-LC3B) in DRG neurons from aged mice with or without overexpression of the indicated Halo-WIP12B construct (mean ± SEM;  $n \geq 17$  neurons from three biological replicates for each condition). \*\*\*\* $p < 0.0001$ ; ns  $p > 0.05$  by Kruskal-Wallis ANOVA test with Dunn's multiple comparisons test. (H) Mean intensity profiles of mCh-ATG5 (red), Halo-WIP12B WT (blue), and GFP-LC3B (green) for productive AVs (mean ± SEM;  $n = 6$  biogenesis events from five neurons from three biological replicates). Vertical dashed line indicates the half-maximum of GFP-LC3B intensity, which was used to align the traces.

DOI: <https://doi.org/10.7554/eLife.44219.019>



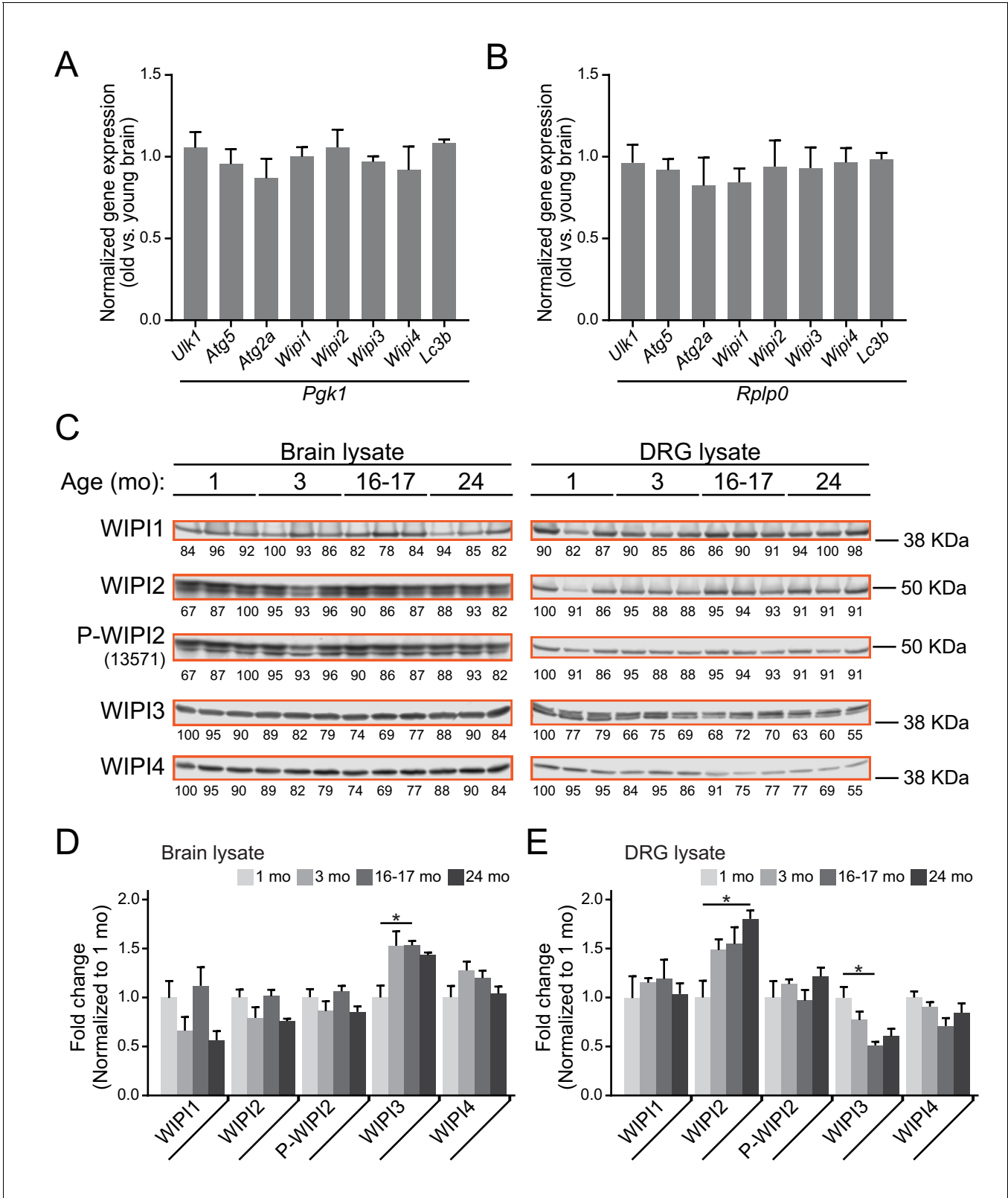


**Figure 6—figure supplement 1.** WIP1 protein and mRNA levels. (A–B) Quantitative real-time PCR of autophagosome biogenesis components in brain from aged versus young adult mice (n = 4 biological replicates for each age). The fold-change in target gene expression level ( $\Delta\Delta C_t$ ) was determined by normalization to two separate reference genes, phosphoglycerate kinase 1 (*Pgk1*) (A) and ribosomal protein, large P0 (*Rplp0*) (B). The official mouse *Wipi3* gene name is *Wdr45b*; the official mouse *Wipi4* gene name is *Wdr45*; and the official mouse *Lc3b* gene name is *Map1lc3b*. (C) Immunoblots of Figure 6—figure supplement 1 continued on next page

*Figure 6—figure supplement 1 continued*

brain or DRG lysates from young, young adult, aged, and advanced mice (n = 3 biological replicates shown for each age). Total protein was used as a loading control (normalization factor indicated below each blot as a percentage). Equal total protein was loaded in each lane for each lysate type (40 µg per lane for brain, 30 µg per lane for DRG). (D–E) Quantification of immunoblots for brain (D) and DRG (E) lysates, normalized first to total protein, then to one mo levels (n = 6 biological replicates for each age, 3 male and three female mice). \*p<0.05 between indicated groups by one-way ANOVA with Tukey's post-hoc analysis; all other groups within one target and lysate type are not significantly different by one-way ANOVA with Tukey's post-hoc analysis.

DOI: <https://doi.org/10.7554/eLife.44219.020>

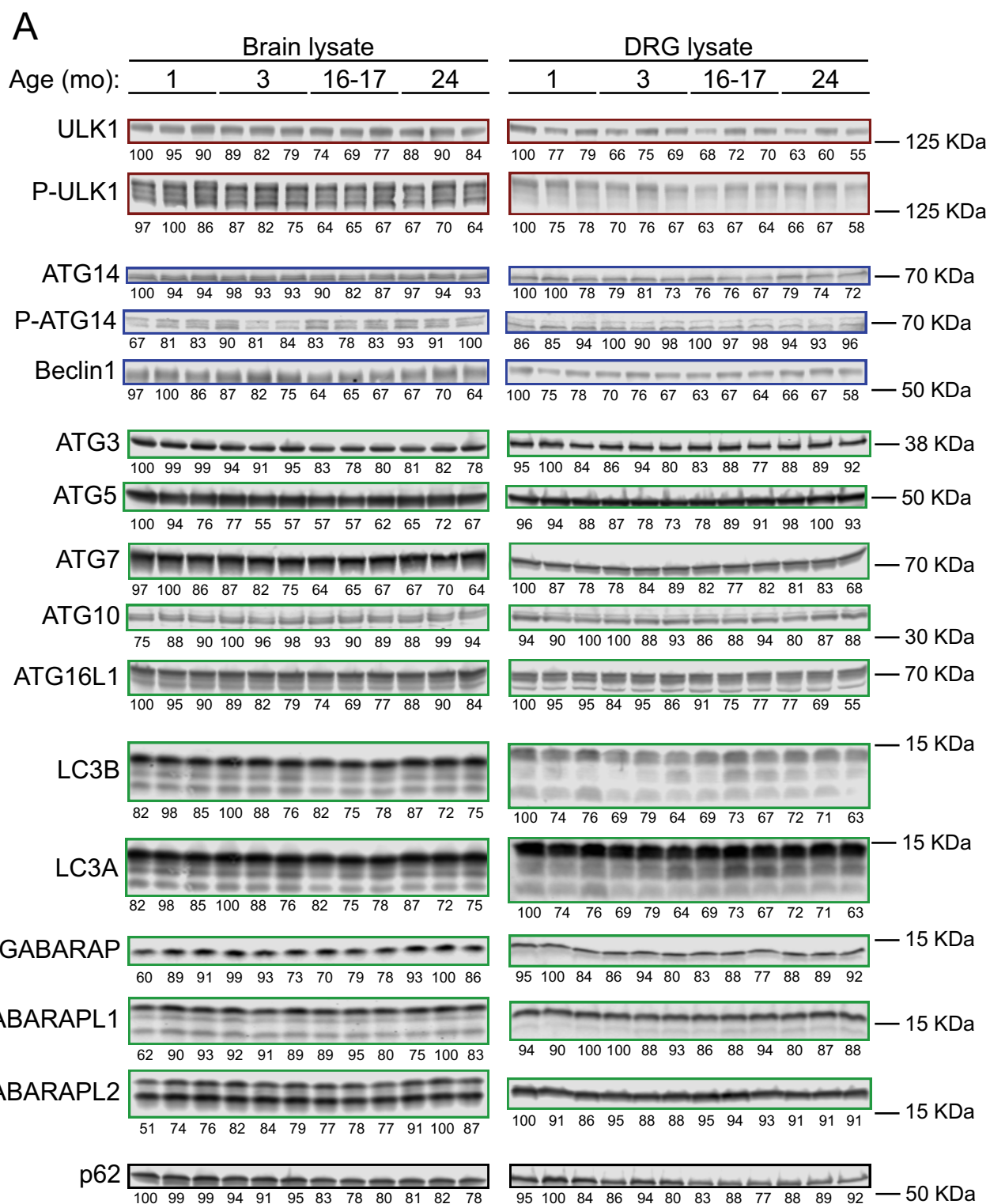


**Figure 6—figure supplement 2.** Autophagy protein levels. (A) Immunoblots of brain or DRG lysates from young, young adult, aged, and advanced aged mice (n = 3 biological replicates shown for each age, blots were repeated on another set of 3 biological replicates for each age). Total protein was used as a loading control (normalization factor indicated below each blot as a percentage). Equal total protein was loaded in each lane for each lysate type (40 µg per lane for brain, 30 µg per lane for DRG).

DOI: <https://doi.org/10.7554/eLife.44219.021>

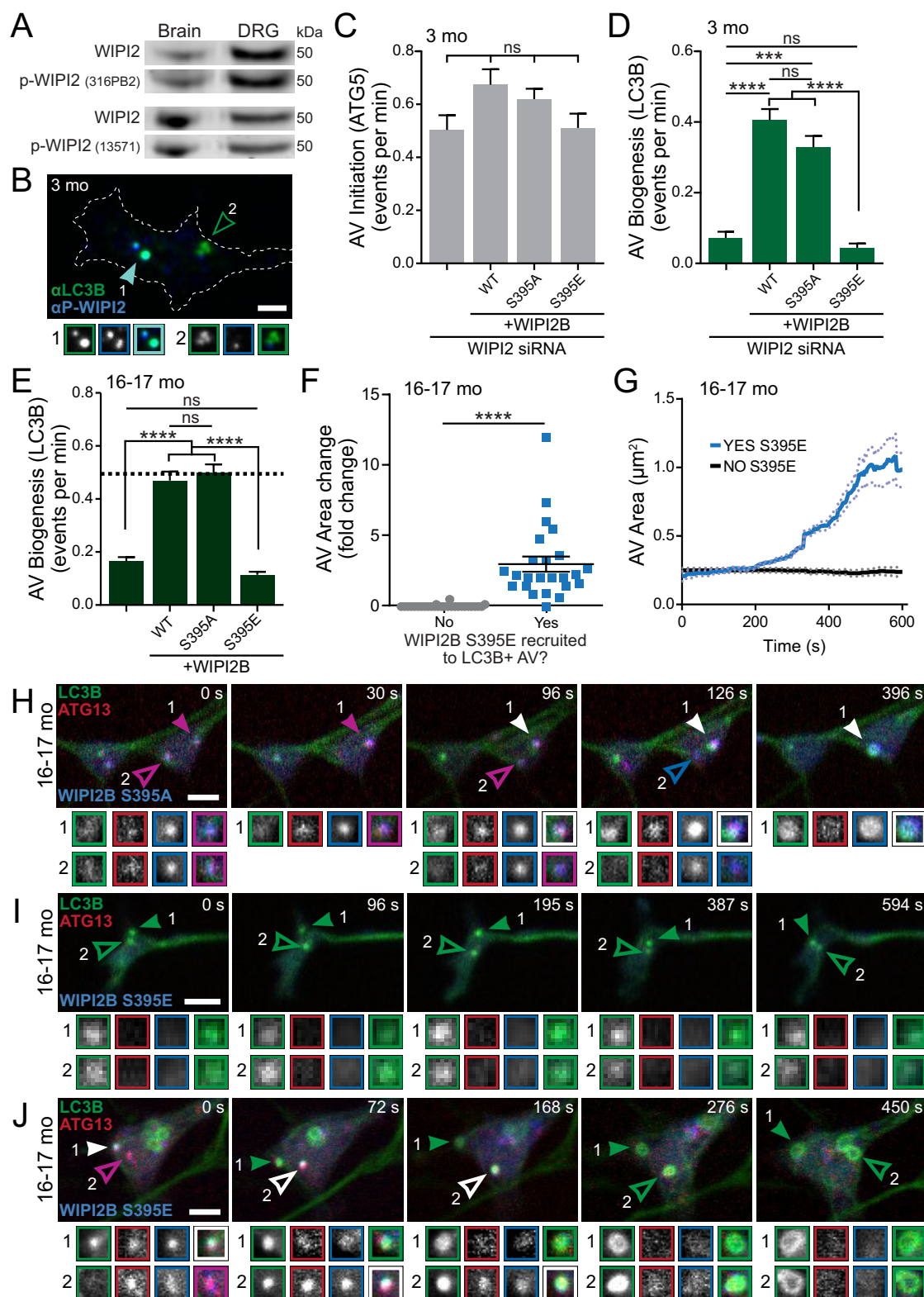


**Figure 7.** Dynamic WIPI2B phosphorylation in neurons is required for autophagosome biogenesis. (A) Immunoblot of whole brain or DRG lysates from aged mice demonstrates p-WIPI2 can be detected with two different phospho-WIPI2 antibodies. (B) Representative maximal projection of a neuron at 3 months, with LC3B (green) and p-WIPI2 (red) co-localizing in an autophagosome (yellow). Figure 7 continued on next page



## Figure 7 continued

immunocytochemistry micrograph of LC3B and phospho-WIP12 in the distal tip of a DRG neuron from a young adult mouse. Arrowheads indicate colocalization state on the AV; solid arrowhead indicates puncta with both proteins, while outlined arrowhead designates a different AV with no phospho-WIP12 colocalized with LC3B. Borders of magnifications of indicated puncta denote channel or colocalization state in merge. Scale bar, 2  $\mu$ m. (C) Quantification of the rate of AV initiation (mCh-ATG5 puncta) in DRG neurons from young adult mice with WIP12 siRNA or WIP12 siRNA with indicated RNAi-resistant Halo-WIP12B constructs (mean  $\pm$  SEM;  $n \geq 17$  neurons from three biological replicates for each siRNA condition). ns (not significant)  $p > 0.05$  by Kruskal-Wallis ANOVA test with Dunn's multiple comparisons test. (D) Quantification of the rate of AV biogenesis (GFP-LC3B puncta) in DRG neurons from young adult mice with WIP12 siRNA or WIP12 siRNA with indicated RNAi-resistant Halo-WIP12B constructs (mean  $\pm$  SEM;  $n \geq 17$  neurons from three biological replicates for each siRNA condition). ns (not significant)  $p > 0.05$ ; \*\*\* $p = 0.0001$ ; \*\*\*\* $p < 0.0001$  by Kruskal-Wallis ANOVA test with Dunn's multiple comparisons test. (E) Quantification of the rate of AV biogenesis (marked with GFP-LC3B) in DRG neurons from aged mice with or without overexpression of the indicated Halo-WIP12B construct (mean  $\pm$  SEM;  $n \geq 23$  neurons from three biological replicates for each condition). \*\*\*\* $p < 0.0001$ ; ns (not significant)  $p > 0.05$  by Kruskal-Wallis ANOVA test with Dunn's multiple comparisons test. Horizontal dashed line indicates rate of AV biogenesis in neurons from young adult mice. (F) Quantification of AV area change with or without recruitment of Halo-WIP12B (S395E) (mean  $\pm$  SEM;  $n \geq 24$  AVs from 14 neurons from three biological replicates). \*\*\*\* $p < 0.0001$  by Mann-Whitney test. (G) Individual AV area profiles were averaged to improve signal-to-noise of GFP-LC3B puncta that were positive (blue) or negative (black) for Halo-WIP12B(S395E) (mean  $\pm$  SEM;  $n \geq 25$  AVs from  $\geq 17$  neurons from three biological replicates). (H) Time series of merge micrographs of GFP-LC3B, mCh-ATG13, and Halo-WIP12B (S395A) in the distal neurite of a DRG neuron from an aged mouse. (I–J) Time series of merged micrographs of GFP-LC3B, mCh-ATG13, and Halo-WIP12B(S395E) in the distal neurite of DRG neurons from aged mice depicting AVs that fail to recruit Halo-WIP12B(S395E) and fail to grow (I) and AVs that do recruit Halo-WIP12B(S395E) and increase in area (J) during the imaging window. Arrowheads indicate colocalization state on the isolation membrane; solid arrowhead follows one punctum, while outlined arrowhead indicates a second AV. Magnified views of denoted puncta are shown below full micrograph; border color represents channel or colocalization state in merge. Retrograde is to the right. Scale bars, 2  $\mu$ m.

DOI: <https://doi.org/10.7554/eLife.44219.023>

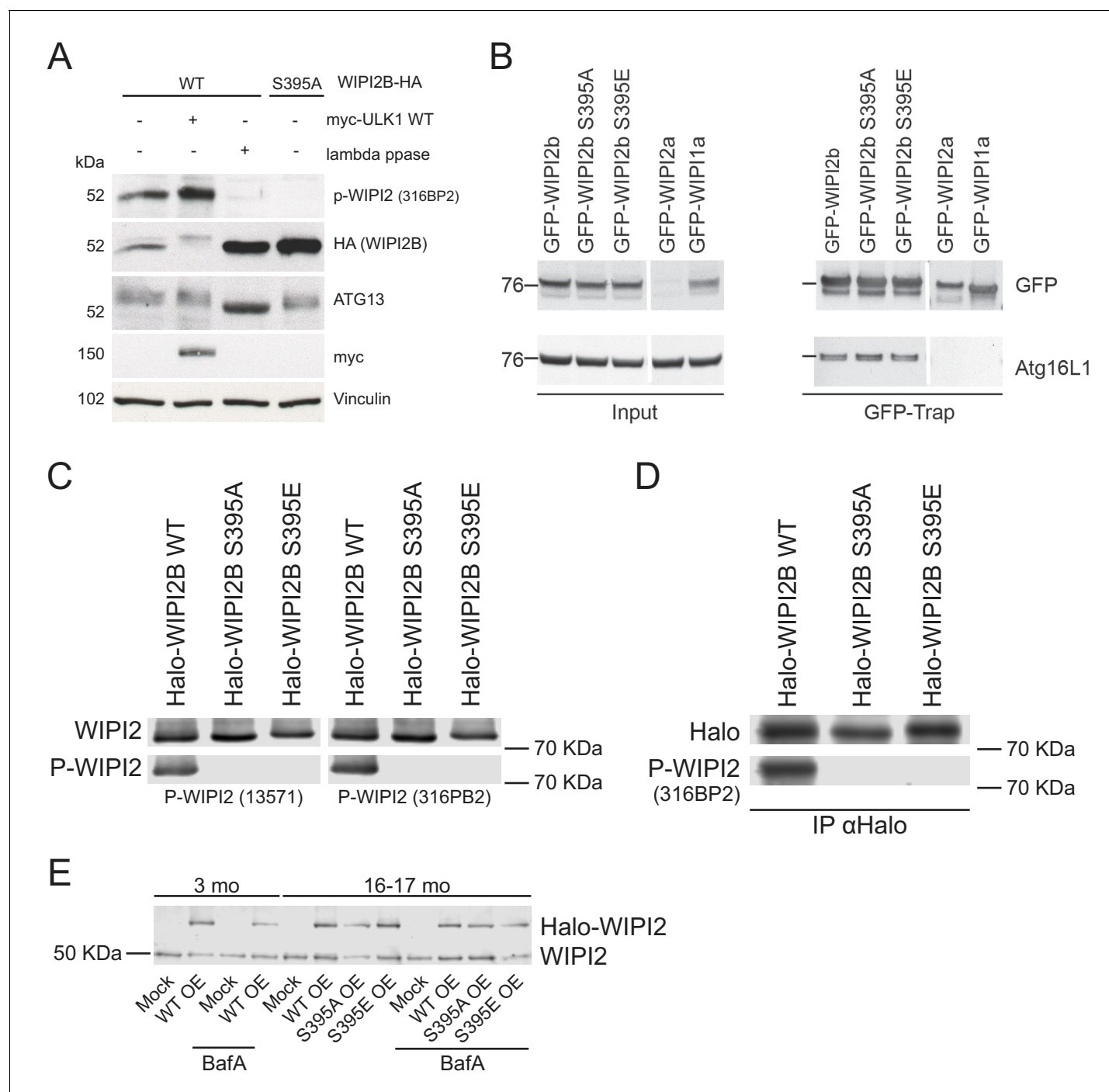


**Figure 7—figure supplement 1.** WIPI2B is phosphorylated at S395. (A) WIPI2 CRISPR KO HEK293A cells were transiently transfected with WIPI2B-HA WT or WIPI2B-HA S395A in combination with either empty vector or myc-ULK1 WT. The cells were lysed and subsequently subjected to lambda phosphatase treatment. Sodium orthovanadate was used as a phosphatase inhibitor in control samples. The samples were analyzed by western blot. Vinculin was used as a loading control. (B) GFP-WIPI2 or GFP-WIPI1A constructs were pulled down using GFP-Trap beads from HEK293 cells expressing GFP-WIPI2B WT, GFP-WIPI2B(S395A), GFP-WIPI2B(S395E), GFP-WIPI2A, or GFP-WIPI1A. ATG16L1 was detected by immunoblotting. (C) HeLa-M cells were transiently transfected with Halo-WIPI2B WT, Halo-WIPI2B(S395A), or Halo-WIPI2B(S395E). The cell lysates were analyzed by western blot. (D) HeLa-M cells were transiently transfected with Halo-WIPI2B WT, Halo-WIPI2B(S395A), or Halo-WIPI2B(S395E). Halo-WIPI2B constructs were pulled down using anti-Halo and detected by immunoblotting.

DOI: <https://doi.org/10.7554/eLife.44219.024>

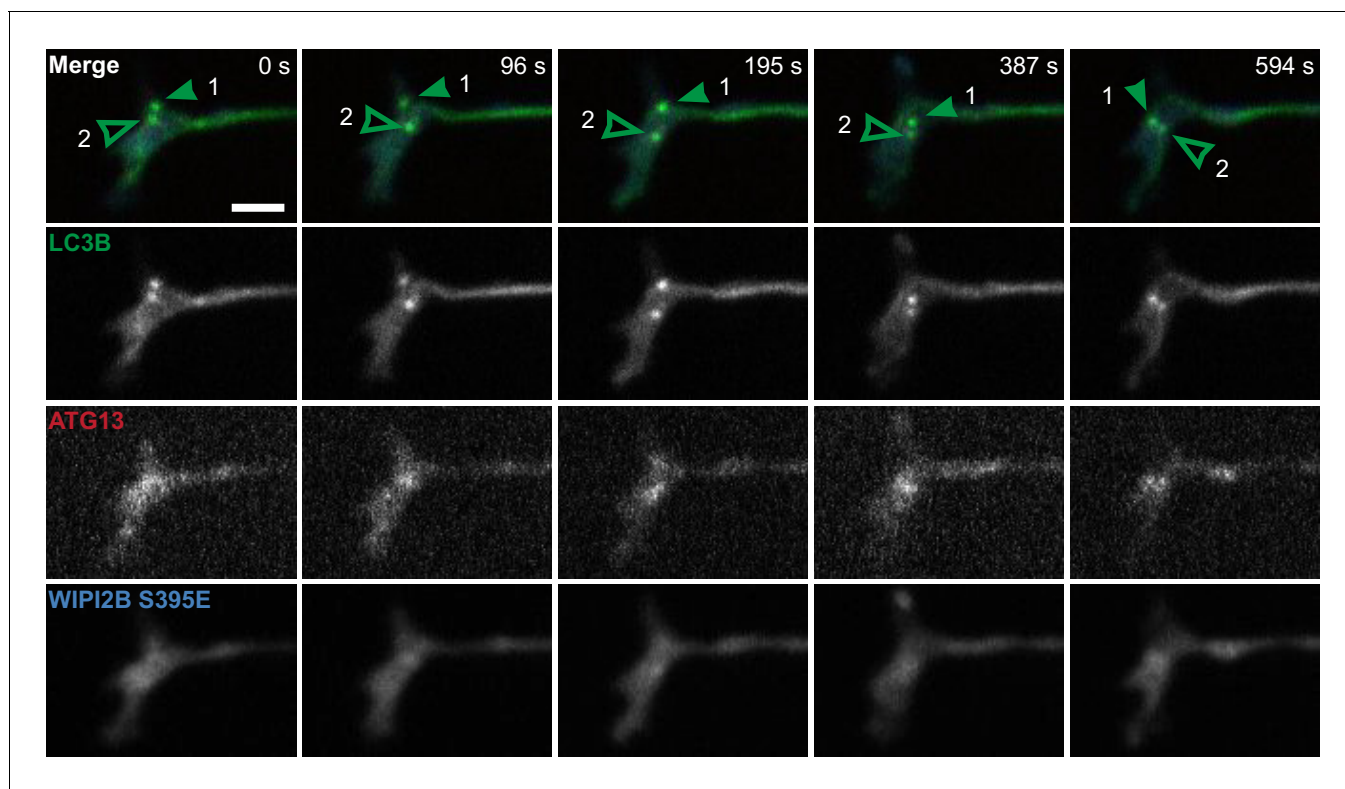


**Figure 7—figure supplement 2.** GFP-LC3B-positive AVs do not enlarge when Halo-WIPI2B(S395E) is not recruited. Full panels of micrographs depicted in **Figure 7I**. Time series of micrographs of GFP-LC3B, mCh-ATG13, and Halo-WIPI2B(S395E) in the distal neurite of DRG neurons from aged mice depicting AVs that fail to recruit Halo-WIPI2B(S395E) and fail to grow during the imaging window. Arrowheads indicate colocalization state on the isolation membrane; solid arrowhead follows one punctum, while outlined arrowhead indicates a second AV. Retrograde is to the right. Scale bars, 2  $\mu$ m.

DOI: <https://doi.org/10.7554/eLife.44219.025>

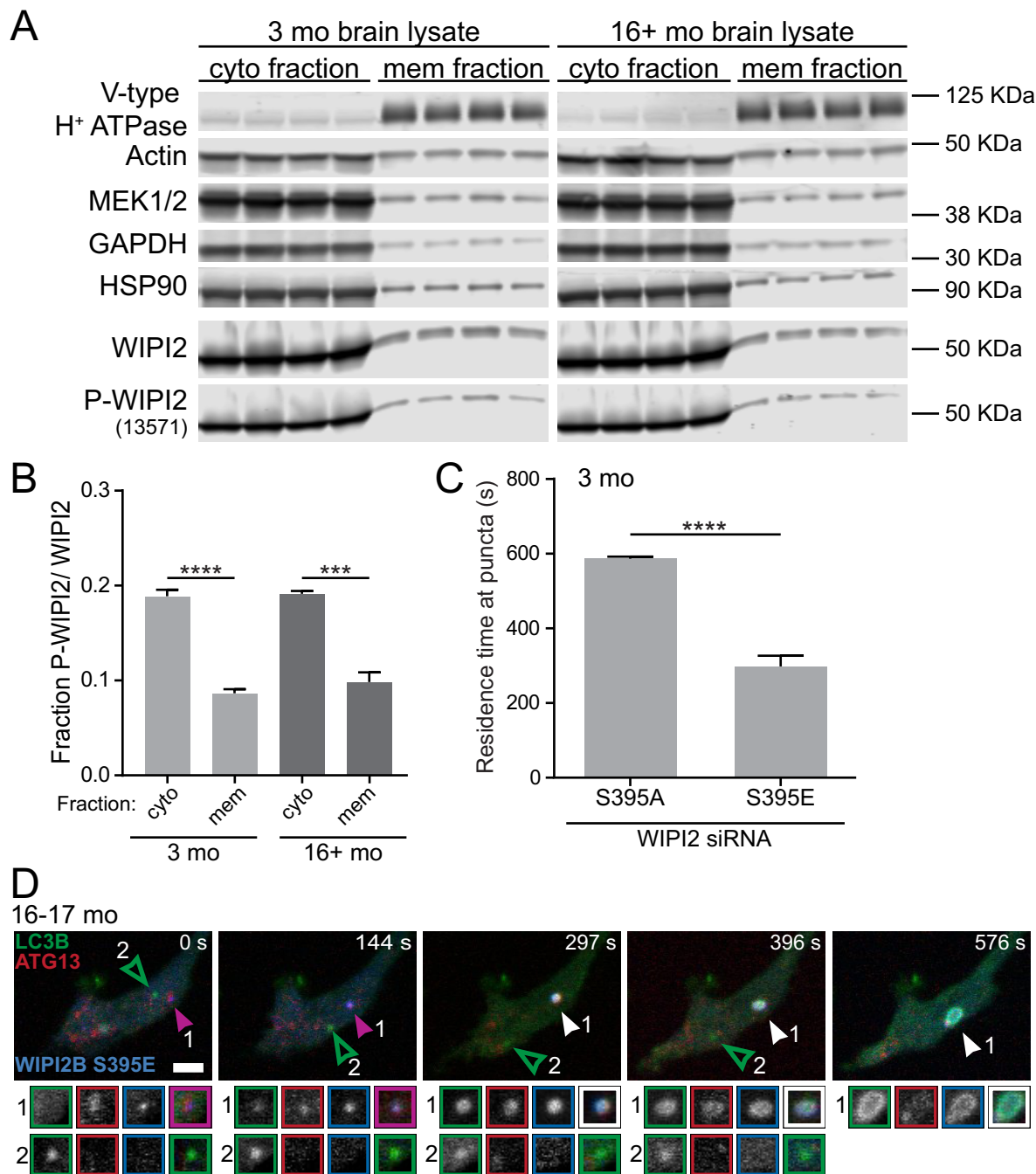


**Figure 8.** Phosphorylation of WIPI2B at serine 395 decreases the affinity of WIPI2B for membranes. (A) Immunoblot of cytosolic and membrane fractions of brain lysates from young adult (left) and aged (right) mice ( $n = 4$  biological replicates for each age). (B) Quantification of the ratio of Phospho-WIPI2 to total WIPI2 in the cytosolic (cyto) and membrane (mem) fractions from the immunoblot in A (mean  $\pm$  SEM;  $n = 4$  biological replicates for each age). \*\*\*\* $p < 0.0001$ ; \*\*\* $p = 0.0001$  by two-tailed unpaired t test. (C) Quantification of the residence time of Halo-WIPI2B(S395A) or SNAP-WIPI2B(S395E) in the distal tips of DRG neurons from young adult mice with WIPI2 siRNA (mean  $\pm$  SEM;  $n = 25$  neurons from three biological replicates). \*\*\*\* $p < 0.0001$  by Mann-Whitney test. (D) Time series of merged micrographs of GFP-LC3B, mCh-ATG5, and Halo-WIPI2B(S395E) in the distal neurite of a DRG neuron from an aged mouse depicting an AV that fails to recruit Halo-WIPI2B(S395E) and fails to grow (open arrowhead) and an AV that does recruit Halo-WIPI2B(S395E) and increases in area (filled arrowhead) during the imaging window in the same DRG distal neurite. Arrowheads indicate colocalization

Figure 8 continued on next page



*Figure 8 continued*

state on the isolation membrane. Magnified views of denoted puncta are shown below full micrograph; border color represents channel or colocalization state in merge. Retrograde is to the right. Scale bar, 2  $\mu$ m.

DOI: <https://doi.org/10.7554/eLife.44219.026>

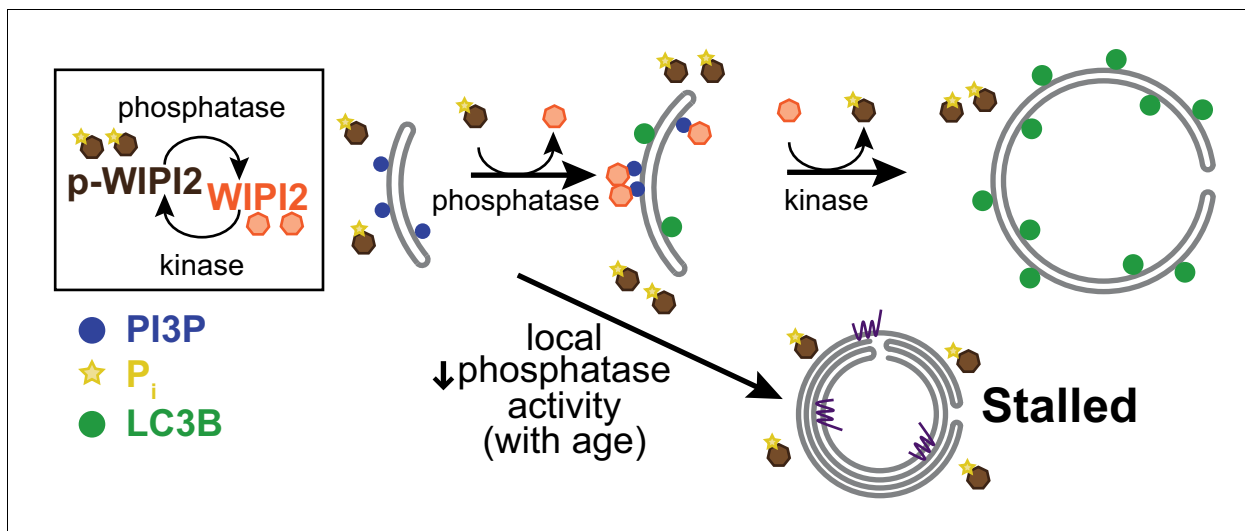


**Figure 9.** Local dynamic phosphorylation of WIPI2B is required for progression through autophagosome biogenesis. Model of how dynamic phosphorylation of WIPI2 and autophagosome biogenesis changes in neurons with aging, characterized by formation of both productive and stalled events.

DOI: <https://doi.org/10.7554/eLife.44219.027>